*Journal of Metals, Materials and Minerals, 36(3), e2423, 2026*

# Graphene-based materials from liquid phase exfoliation of graphite using mangosteen-peel extract: Experiments and molecular simulation

Piyaphat THEPPHOT[1], Narissara KARAKATE[1], and Panu DANWANICHAKUL[1,*]

[1] *Department of Chemical Engineering, Thammasat School of Engineering, Faculty of Engineering, Thammasat University, 99 Moo 2, Paholyothin Rd., Klong-Nung, Klong-Luang, Pathumthani, 12120, Thailand*

***Corresponding author e-mail**: dpanu@engr.tu.ac.th

**Received date:**
4 June 2025
**Revised date:**
18 March 2026
**Accepted date:**
5 June 2026

**Keywords:**
Graphene;
Graphite exfoliation;
Mangosteen peel;
Condensed tannin;
Molecular simulation

**Abstract**

The conventional Hummers method for graphene production requires large quantities of hazardous chemicals, causing environmental impacts and sustainability concerns. This study investigated mangosteen-peel extract as a natural alternative in liquid phase exfoliation of graphite, exploiting the structural similarity between condensed tannins and graphite, which enables π–π interactions. Four exfoliation processes were studied: shear force via a homogenizer (9,500 rpm and 14,000 rpm for 41 min), sonication using an ultrasound bath (200 W and 400 kHz) for 2 h and 3 h at 50°C and their sequential combinations. The results confirmed successful graphite exfoliation yielding samples with I2D/IG ratios of 0.51 to 0.55 which are comparable to commercial graphene-based products. This was also verified by the increased specific surface area using BET analysis and TEM imaging showing structures with five and more layers. The yields of exfoliated products from all processes were 4.39% to 8.5%. Lastly, Molecular dynamics simulation revealed that when changes of van der Waals interactions were considered, increasing condensed tannin concentration exerted the greatest effect on graphite exfoliation, followed by increases in pressure and temperature. This research demonstrates the potential use of mangosteen-peel extract as an environmentally friendly alternative for multi-layer graphene production.

## 1. Introduction

Nanomaterials have recently played an important role in many industries. Due to their miniature scale of 1 nm to 100 nm, nanomaterials possess unique physical, chemical, and biological properties. This leads to the study of various types of nanomaterials, including graphene, a two-dimensional nanomaterial. Theoretically, graphene is a material composed of a single layer of carbon atoms linked together by a covalent bond and arranged in a hexagonal close-packed plane. Material consisting of two or more layers are classified as graphene-based material. It has excellent electrical conductivity, thermal conductivity, strength and flexibility. Therefore, graphene-based materials have been applied as fillers to enhance the polymer properties [1] and used as an excellent supercapacitor [2]. Both graphene-based materials and other graphene derivatives such as two-dimensional graphitic carbon nitride (g-$C_3N_4$) have been investigated for electronic applications [3,4].

The production of graphene-based materials can be accomplished through either bottom-up or top-down processes. In the former, carbon atoms undergo a reaction to form graphene-based materials such as via chemical vapor deposition. However, this method is complex and expensive. The latter is more widely studied in both solid and liquid phases, starting with graphite, whose layers are held together by weak intermolecular Van der Waals force. In liquid phase exfoliation, graphite is dispersed in a liquid and the suspension is then disturbed by external forces such as shear force from a probe homogenizer or ultrasound waves in an ultrasound bath.

A conventional top-down process is called Hummers method, in which graphite is reacted with various strong oxidizing agents in liquid phase to form graphene oxide (GO). However, oxygen-containing functional groups of graphene oxide reduce its electrical conductivity. Therefore, strong reducing agents must be used to partially remove oxygen atoms and the product is called reduced-graphene oxide (rGO). Despite the high yield, this method utilizes numerous hazardous chemicals that pose a threat to the environment and human health.

Nowadays, more environmentally friendly and sustainable processes have gained increasing attention. The green exfoliation using physical means to separate graphite layers has been investigated. The extracts from plants and agricultural wastes have been used in liquid exfoliations to facilitate exfoliation because these hydrophilic organic substances could increase wettability of graphite surfaces, leading to enhanced graphite dispersion in liquid and the interactions between organic molecules and graphite surfaces could weaken the van der Waals attraction between graphite layers. Upon applying shear force or ultrasound to the liquid, graphite layers could separate from one another and the exfoliation happens.

Mangosteen is an important economic crop in Thailand. In 2023, the mangosteen production in Thailand was approximately 271,000 MT [5]. A mangosteen fruit contains approximately 31% pulp and 69% peel [6]. Since only the pulp is edible, a large amount of waste was generated from the discarded peels. Mangosteen peels were extracted by methylene chloride and found containing xanthone derivatives, primarily α-mangostin and γ-mangostin of 33.24 $mg \cdot g^{-1}$ and 8.61 $mg \cdot g^{-1}$

dried peel, respectively [7]. Additionally, the peels contain 7.14% condensed tannins (or approximately 71.4 mg·g$^{-1}$ dried peel) [8]. Due to the anti-inflammatory, antibacterial and antioxidant properties of these polyphenol compounds, the peels have been used in diet supplementary, pharmaceuticals, and cosmetics.

A research work investigated the use of curcumin in ethanol solution in liquid phase exfoliation of graphite together with sonication. It was hypothesized that the ring structures in curcumin could form π–π interactions with graphite layers, facilitating the exfoliation [9]. In alignment with this hypothesis, the ring structures of other polyphenol compounds should form π–π interactions with graphite layers. Because condensed tannins in mangosteen peel contain abundant phenol groups in its structure, it is of interest to apply the mangosteen-peel extract in graphite exfoliation.

Therefore, this research aims to study the liquid phase exfoliation of graphite to obtain graphene-based material by using mangosteen-peel extract together with external forces including shear force from a homogenizer and impact pressure from bubbles collapse in an ultrasound bath. In addition, the sequential combinations of both processes were also studied. Moreover, the interactions between a condensed tannin molecule and a sample of graphite were observed in the molecular dynamic simulation via BIOVIA Materials Studio program.

## 2. Experimental

### 2.1 Materials

Graphite powder (particle size less than 50 μm) was purchased from Merk & Co., Mangosteen peel powder was supplied from Baanplaina, an online store in Thailand. Graphene-based materials (the thickness of 6 nm to 8 nm and the width of 5 μm) was purchased from TCI. Tannic acid was supplied by Sigma-Aldrich. Gallic acid with 98% purity was purchased from SRL and sodium dodecyl sulfate (SDS) was provided by Ajax Finechem. Folin-Ciocalteu reagent was purchased from Loba Chemie and Sodium carbonate with 99.5% purity and AR grade was supplied by KEMAUS.

### 2.2 Determination of total phenolic content (TPC) and total tannin content (TTC) of mangosteen-peel extract

Firstly, the mangosteen-peel extract was prepared by extracting 5 g of mangosteen peel powder with 100 mL of hot water at 80°C. The mixture was stirred and allowed to stand for 10 min prior to filtration. The extract was then diluted with different volume ratios of the extract and distilled water and these were analyzed for TPC and TTC.

Next, a calibration curve was constructed using gallic acid standards [10] prepared at different concentrations ranging from 50 mg·L$^{-1}$ to 2000 mg·L$^{-1}$. 0.1 mL of each gallic acid solution was mixed with 0.75 mL of Folin-Ciocalteu reagent and 7.5 mL of distilled water. After mixing, 0.75 mL of 10 %w/v sodium carbonate solution was added. The mixture was shaken with a vortex mixer and incubated at room temperature for 90 min. The absorbance of the mixture was measured at 725 nm using a UV-Vis spectrophotometer. Total phenolic content (TPC) was expressed as gallic acid equivalence (GAE), while total tannin content (TTC) [11] was determined using tannic acid standards at different concentrations instead and the results were expressed as tannic acid equivalence (TAE).

### 2.3 Graphite exfoliation with mangosteen-peel extracts

The same concentration of graphite was fixed in every experiment at 25 mg·mL$^{-1}$ (total of 2.5 g graphite in total volume of 100 mL). However, the system size was different for using the homogenizer and the ultrasonic bath. The experiments were done in triplicate for each treatment to obtain the average values of the process yields.

#### 2.3.1 Single-step process

For homogenization, 1.25 g of graphite powder was mixed with 50 mL of mangosteen-peel extract solution (Section 2.2) in each of the two beakers, the suspensions were treated at 9,500 rpm and 14,000 rpm for 41 min, then aliquoted into glass bottles (10 mL each) and allowed for 2 h at room temperature. For sonication, 0.25 g of graphite powder was mixed with 10 mL mangosteen-peel extract solution in 10 glass bottles and subjected to ultrasonic treatment (40 kHz and 200 W) at 50°C for 2 h and 3 h. After that all were left for 2 h at room temperature for sedimentation of large particles.

Following different treatment above, 7 mL of supernatant was sampled and the suspended solid was collected by centrifugation at 10000 rpm for 20 min. The solids were then washed sequentially with SDS solution and distilled water and dried to constant weight. The resulting products were labeled as GP-H95 and GP-H140 for samples homogenized for 41 min at 9500 rpm and 14,000 rpm, respectively and GP-U2 and GP-U3 for samples sonicated for 2 h and 3 h at 50°C, respectively.

#### 2.3.2 Two-step process

Using the sequential combination process described in Section 2.3.1, eight products were obtained. After that all were left for 2 h at room temperature for sedimentation of large particles. As in 2.3.1, the products were collected, washed and dried to constant weight. They are designated as GP-H95U2, GP-H95U3, GP-H140U2, and GP-H140U3 for samples homogenized first and then sonicated and GP-U2H95, GP-U2H140, GP-U3H95, and GP-U3H140 for samples sonicated first and then homogenized. For example, GP-H95U2 is the product obtained from being homogenized at 9500 rpm for 41 min and then sonicated at 50°C for 2 h.

### 2.4 Characterization of the exfoliated graphite

#### 2.4.1 Yield percentage of graphite exfoliation

The yield was estimated to obtain the quantities of products from totally twelve different treatments according to Equation (1).

$$\%\ Yield = (W_1/W_2) \times 100 \quad (1)$$

Where, $W_1$ is the weight of dried suspended solid collected from supernatant and $W_2$ is the weight of precursor graphite used in each experiment.

It should be noted that the suspended solid might include the unexfoliated graphite which are fine enough to suspend in the liquid after 2 h sedimentation. Therefore, to check the quality of the obtained solid, more characterizations are needed. Both the quantity and the quality of the graphene-based products were of interest and importance.

#### 2.4.2 Raman spectroscopy

Raman spectroscopy results of the chosen exfoliated graphite including GP-H140, GP-U3, GP-H140U3 and GP-U3H140 were obtained using a dispersive Raman microscope (Brand: Bruker Optics, Model: Senterra) with the laser wavelength at 523 nm, the laser power at $20 \times 10^{-3}$ W and wavenumber from 4500 $cm^{-1}$ to 700 $cm^{-1}$. The measurement followed the standard methods, ASTM: E1693 and ASTM: E1840.

#### 2.4.3 Fourier transform infrared spectroscopy (FTIR)

The prepared graphene-based materials and reference samples, including graphite precursor, mangosteen-peel powder and exfoliated graphite (before and after washing with SDS solution and distilled water) were analyzed using Fourier transform infrared spectroscopy (Brand: Perkin Elmer, Model: Frontier). Small quantities of powdered samples were placed on the diamond crystal (2 mm in diameter) and compressed using a steel anvil. FTIR spectra were recorded in the range of 4000 $cm^{-1}$ to 400 $cm^{-1}$ with 4 scans and a force gauge setting of 85.

#### 2.4.4 BET specific surface area analyzer

Surface area analysis of finely ground samples of 0.15 g was performed using BET specific surface area analyzer (Brand: Quantachrome, Model: Autosorb-IQ-MP/KR. Nitrogen adsorption isotherms were measured at –195.8°C using standard BET parameters: molecular weight 28.013 $g \cdot mol^{-1}$, effective diameter 3.54 Å, cross-sectional area 16.20 $Å^2$, and liquid density 0.808 $g \cdot cm^{-3}$. The samples were degassed at 250°C overnight. The results including specific surface area, total pore volume and average inter-sheet spacing of exfoliated graphite were determined.

#### 2.4.5 Transmission Electron Microscopy (TEM)

Three exfoliated graphite samples (GP-H140, GP-U3, GP-U3H140) were dehydrated with ethanol and mounted on copper grids, stained with heavy metals for contrast enhancement and examined using transmission electron microscopy (Brand: JEOL, Model: JEM-2010) equipped with a $LaB_6$ thermionic electron source operating at $200 \times 10^3$ eV.

### 2.5 Molecular dynamic simulation (MD)

MD simulations were performed using BIOVIA Materials Studio program**.** Initially, molecular structures of condensed tannin, water and an 8 layer graphite system were constructed. An amorphous liquid system containing 1 molecule of condensed tannin and 1219 molecules of water (equivalent to 7 wt% of condensed tannin in water) was generated and geometrically optimized before MD simulation. The system was equilibrated for 200,000 picoseconds under isothermal-isobaric (NPT) ensemble conditions. Subsequently, a layered system was constructed with the amorphous liquid phases (layer 1 and layer 3) sandwiched with the 8 layer graphite structure (layer 2).

Following geometry optimization, comprehensive MD simulations were executed using the Forcite module under canonical (NVT) ensemble conditions at 25°C and $1.013 \times 10^5$ Pa to investigate the potential energy. The COMPASS force field was selected because it provides reliable descriptions of condensed-phase organic and carbon-based systems, particularly non-bonded interactions such as van der Waals and electrostatic interactions, which are critical in graphite exfoliation processes. Ewald summation was employed for both electrostatic and van der Waals interactions to improve the accuracy of long-range interaction calculations in the layered graphite system. A cutoff distance of 12 Å was selected for van der Waals interactions, which is within the commonly accepted range for molecular dynamics simulations of graphite-based and condensed-phase systems. This value provides a reasonable balance between computational efficiency and calculation accuracy. Since the interlayer spacing of graphite is approximately 3.35 Å, the selected cutoff distance is sufficiently large to capture interlayer interactions, tannin–graphite interactions, and solvent effects. In addition, the use of Ewald summation for van der Waals interactions further improves the accuracy of long-range interaction calculations in the layered graphite system.

To study the energy effect, various parameters were investigated including (1) temperature increase from 25°C to 50°C at a constant pressure of $1.013 \times 10^5$ Pa, (2) pressure increase from $1.013 \times 10^5$ to $2.026 \times 10^5$ Pa at a constant temperature of 50°C and (3) variation in the number of condensed tannin molecules from 0 molecule, 1 molecule and 2 molecule, where 0 molecule represents an amorphous system of pure water. All experiments were conducted in duplicate and the resulting energy values were averaged. Even though the simulated system is quite small and does not represent the actual phenomena of graphite exfoliation, the results of van der Waals energy changes is enough to reflect the effect of temperature, pressure and number of tannin molecules.

## 3. Results and discussion

### 3.1 Total phenolic content (TPC) and total tannin content (TTC)

The TPC and TTC analyses are based on a redox reaction involving electron transfer between phenolic compounds in gallic acid and in tannic acid, respectively, and tungsten ($W^{6+}$) and molybdenum ($Mo^{6+}$) ions in the Folin-Ciocalteu reagent. When $W^{6+}$ and $Mo^{6+}$ accept electrons from phenolic compounds, the reaction mixture is incubated at room temperature until equilibrium is reached. The solution undergoes a color change to form tungsten blue and molybdenum blue complexes. Sodium carbonate was added to accelerate the reaction and achieve equilibrium more rapidly.

The extract was diluted to different concentrations with different volume percentage of the extract ranging from 5 to 100. Each solution was checked for TPC and TTC. Figure 1 revealed that the correlation coefficient ($R^2$) approached unity for both TPC and TTC, demonstrating linear relationship between TPC and TTC with extract concentrations. This implies that the interference of extract color, especially at a high concentration, on the measurement of TPC and TTC is negligible.

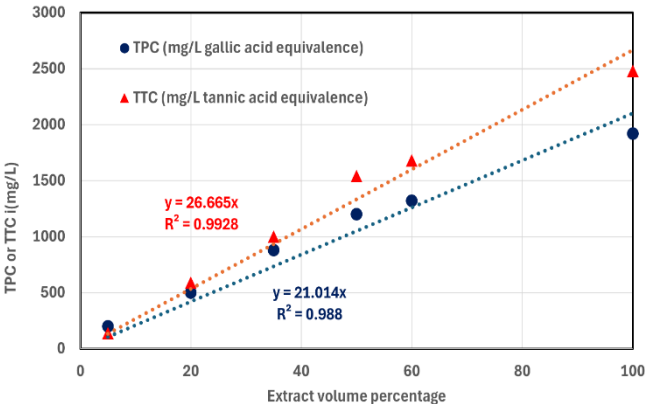


**Figure 1.** Relationship between extract volume percentage in dilution and TPC (red line) and TTC (blue line)

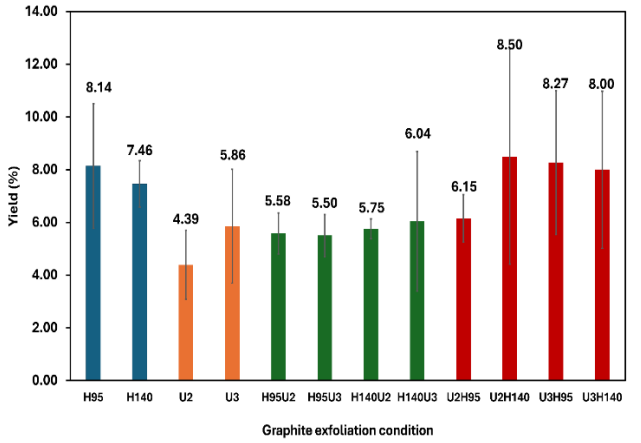


**Figure 2**. Yield percentages of all exfoliated graphite samples from single-step and two-step processes.

The undiluted extract (extract volume percentage of 100) demonstrated the highest values, with gallic acid equivalence and tannic acid equivalence of 1920 mg·L$^{-1}$ GAE (or 38.4 mg·g$^{-1}$ GAE) and 2480 mg·L$^{-1}$ TAE (49.6 mg·g$^{-1}$ TAE), respectively. The former value was higher than those previously reported for water-extracted (7.2 mg·g$^{-1}$ GAE), 50% ethanol-extracted (12.4 mg·g$^{-1}$ GAE) and 50% acetone-extracted (10 mg·g$^{-1}$ GAE) using 25 mL of solvent and 1.25 g of peels [12]. In later experiments, the undiluted extract solution was used to exfoliate graphite.

Among the compounds present in mangosteen peel, condensed tannins are expected to play the dominant role in graphite exfoliation because their multiple aromatic rings can strongly interact with graphite surfaces through π–π interactions. Xanthones and other polyphenolic compounds may also contribute to the exfoliation process due to their aromatic and conjugated structures, which are capable of forming π–π interactions with graphite layers but xanthones cannot be extracted well with water. In contrast, sugars and organic acids are less likely to directly promote exfoliation because they lack conjugated aromatic π-systems, although they may indirectly affect the process by influencing the wettability, dispersion stability, and physicochemical properties of the system. Therefore, in the following discussion and in Section 3.4 the molecular dynamic simulation, tannin is in focus.

## 3.2 Yield of the process

The yield of the process indicated the capability of applying the external forces and natural extracts for graphite exfoliation. They demonstrated the efficiency of utilizing natural waste materials while reducing chemical usage in industrial graphene-based material production. The yields of exfoliated graphite samples from all conditions are shown in Figure 2 as the average values with deviations.

Figure 2 shows that single-step homogenization (GP-H95 and GP-H140) resulted in a decrease in yield from 8.14% to 7.46% at higher shear forces possibly due to tannin-graphite adsorption, which caused π-π interactions that promoted simultaneous exfoliation and graphite precipitation, resulting in the fewer amount of suspended solid after 2 h sedimentation. Single-step ultrasonication (GP-U2 and GP-U3) resulted in increased yield from 4.39% to 5.86% with longer sonication time. Ultrasonication creates small air bubbles whose breakages generate high pressure forces that could impact and move graphite edges during exfoliation, known as wedge effect [13]. This impact could reduce tannin adsorption on graphite surfaces compared to homogenization systems, resulting in smaller effect of adsorption. These yields exceeded the reported values of 3% when using sodium cholate solution via homogenization at 16500 rpm for 2 h [14] and 1% curcumin in ethanol solution via ultrasonication at 1080 W for 4 h [9].

It was expected that synergistic effects should arise when the combinations of two or more processes produce effects greater than the sum of their individual effects [15]. However, in our case, Figure 2 shows that the sequential combinations of homogenization and ultrasonication revealed no synergistic effect of the two processes because only slight increases in yield were observed. It is thought that adsorption of many large tannin molecules on graphite surfaces play a very important role in both exfoliation and precipitation. As discussed above, homogenization seemed to promote a higher degree of adsorption than sonication, if the process began with homogenization, the adsorption on graphite surfaces might obstruct the effect of impact from pressure forces in later step of sonication, leading to yield percentages even smaller than from homogenization alone (5.58% to 6.04%). When beginning with ultrasonication, the exfoliation occurred already at some degrees with some edges being wedged. If it was followed with homogenization, the shear forces could move the wedged edges apart from one another, leading to the slightly increased yield (6.18% to 8.50%. This absence of synergy is likely resulted from competition between precipitation and exfoliation mechanisms, which both were originated with adsorption.

## 3.3 Characterization of exfoliated graphite

### 3.3.1 Raman spectroscopy results

The Raman effect is the inelastic scattering of light [16]. Raman spectroscopy was used to examine the intrinsic properties of exfoliated graphite, precursor graphite and commercial graphene-based product. The x-axis and y-axis represent Raman shift and intensity, respectively. Raman shift indicates energy differences between incident and scattered light, enabling molecular identification through unique characteristic values. The D-peak indicates structural defects within the sample. The G-peak corresponds to $sp^2$ carbon vibrations and the 2D-peak reflects intrinsic properties of the sample. These peaks appear at

1350 $cm^{-1}$, 1580 $cm^{-1}$, and 2720 $cm^{-1}$, respectively [17]. The $I_D/I_G$ ratio correlates with the number of structural defects. The $I_{2D}/I_G$ ratio inversely correlates with the number of layers; higher values indicate fewer layers. Raman spectroscopy results of the chosen exfoliated graphite samples (GP-H140, GP-U3, GP-H140U3 and GP-U3H140) are illustrated in Figure 3 and reported in Table 1.

The $I_D/I_G$ ratios of the precursor graphite and the commercial graphene-based products are 0.26 and 0.24, respectively. This indicates that graphite contains more defects than graphene-based materials. The defects can be classified to the edge defects and structure defects from the formation of functional groups as of graphene oxide. Therefore, it is possible for this ratio to increase as the number of edge defects increases upon exfoliation with shear force and pressure force in the ultrasonic bath. The $I_D/I_G$ ratios of all exfoliated graphite samples ranged from 0.36 to 0.49, higher than graphite precursors because of more edge defects. However, the values are lower than 0.63 and 0.62 of the samples treated using skim natural rubber latex via both homogenization at 5400 rpm for 20 min and ultrasonication at 200 W for 2 h, respectively [18].

It is shown that homogenization produced samples with higher $I_D/I_G$ ratios than ultrasonication. The high shear forces from homogenization created more defects than the wedge effects from bubble collapse in the ultrasonic bath. Table 1 also shows that when using sequential combination process, the $I_D/I_G$ ratios are obviously greater when compared with single-step process due to the samples are subjected to prolonged external forces.

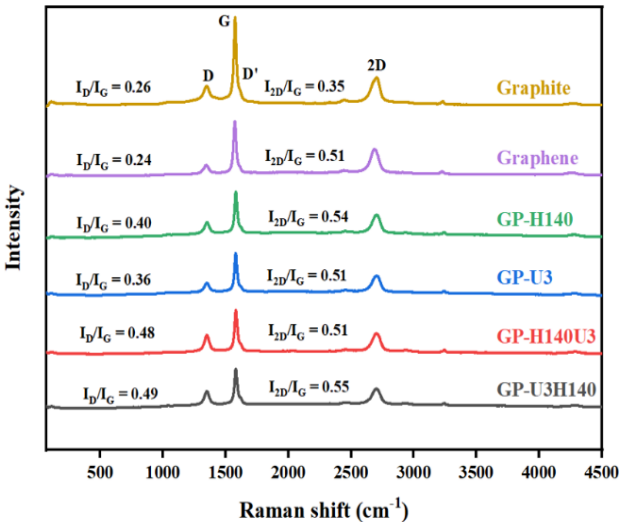


**Figure 3**. Raman spectra of the chosen exfoliated are compared with the those of precursor graphite and the commercial graphene-based product.

In addition, the $I_{2D}/I_G$ ratios of all exfoliated graphite samples range from 0.51 to 0.55, which were higher than the graphite precursor (0.35) and comparable to the commercial graphene-based product (0.51). This indicates that graphite exfoliation was successful in producing graphene-based materials with the number of layers comparable to the commercial graphene-based product. The reduction of number of layers was clearly seen in TEM micrographs in Section 3.3.4.

### 3.3.2 FTIR spectra results

FTIR is an analytical technique based on infrared radiation absorption by molecules, causing bond vibrations at specific frequencies. This allows identification of functional groups in molecular structures. In this research, FTIR spectra was used to confirm the adsorption of molecules of the extracts on graphite surfaces, thereby detecting residues in exfoliated samples by comparing peak position differences between graphite precursor, mangosteen peel powder and exfoliated graphite samples (before and after washing with sodium dodecyl sulfate).

The FTIR analysis (400 $cm^{-1}$ to 4000 $cm^{-1}$) in Figure 4 depicts characteristic absorption bands in mangosteen peel powder (blue lines). Main peaks were identified for C-O stretching (1100 $cm^{-1}$ to 1300 $cm^{-1}$), aromatic substitution (600 $cm^{-1}$ to 1300 $cm^{-1}$), C-C in aromatic ring (1400 $cm^{-1}$ to 1600 $cm^{-1}$), C=O stretching (1703 $cm^{-1}$), conjugated alkene (1604 $cm^{-1}$), aromatic C-H bending aromatic compound (1650 $cm^{-1}$ to 2000 $cm^{-1}$), and O-H stretching (2500 $cm^{-1}$ to 3300 and 3230 $cm^{-1}$ to 3350 $cm^{-1}$) [19-21]. These spectral features indicate the presence of functional groups characteristic of condensed tannins in mangosteen peel [21]. As a reference, the spectrum of tannic acid powder was also shown (orange line) which was similar to that of mangosteen peel powder but the peaks were more pronounced due to its high purity.

Figure 4 also exhibits that GP-H95 before washing has a spectrum similar to that of mangosteen peel powder with notable blueshifts in key peaks including aromatic substitution (1278 $cm^{-1}$ to 1283 $cm^{-1}$), C-C in aromatic ring (1516 $cm^{-1}$ to 1519 $cm^{-1}$), C-H bending aromatic compound (1729 $cm^{-1}$ to 1730 $cm^{-1}$) and O-H (2927 $cm^{-1}$ to 2937 $cm^{-1}$). These spectral shifts confirm that mangosteen peel components are noncovalently interacting with exfoliated graphite probably through π-π interactions between the aromatic rings of condensed tannins and the graphite surface [22]. After washing, GP-H95 has a spectrum similar to those of graphite and commercial graphene but some noise peaks near the wave number of 400 $cm^{-1}$ were more observed, implying that washing is effective enough with probably a small number of residual molecules on the surfaces. In comparison with GP-H95, the spectrum of exfoliated graphite GP-U2 after washing is similar with fewer noise peaks near the wave number of 400 $cm^{-1}$, implying that

**Table 1**. Raman spectra results including primary peak position, intensities and the corresponding ratios of peak intensities of the exfoliated graphite samples.

| Sample | D-peak [$cm^{-1}$] | $I_D$ | G-peak [$cm^{-1}$] | $I_G$ | 2D-peak [$cm^{-1}$] | $I_{2D}$ | $I_D/I_G$ | $I_{2D}/I_G$ |
|---|---|---|---|---|---|---|---|---|
| Graphite | 1349.52 | 3269.10 | 1576.27 | 12581.49 | 2703.83 | 4444.82 | 0.26 | 0.35 |
| Commercial graphene | 1344.39 | 1824.28 | 1570.11 | 7740.24 | 2689.47 | 3973.68 | 0.24 | 0.51 |
| GP-H140 | 1351.57 | 2747.03 | 1584.13 | 6878.32 | 2701.78 | 3738.54 | 0.40 | 0.54 |
| GP-U3 | 1346.44 | 2267.40 | 1577.29 | 6290.32 | 2699.72 | 3218.17 | 0.36 | 0.51 |
| GP-H140U3 | 1349.52 | 3061.69 | 1582.42 | 6426.99 | 2703.83 | 3261.74 | 0.48 | 0.51 |
| GP-U3H140 | 1347.47 | 2928.98 | 1581.40 | 5929.82 | 2701.78 | 3243.92 | 0.49 | 0.55 |

a fewer amount of tannin molecules adsorbed on graphite surfaces, as discussed earlier in Section 3.2 that adsorption in sonication case was less pronounced than in homogenization case. This observation is consistent with the analysis described in the yield percentage. Furthermore, exfoliated graphite samples before and after SDS washing showed that extract residues slightly remained slightly despite the cleaning process. This finding is consistent with another study using tannic acid solutions for graphite exfoliation and reporting similar residual compounds. However, further tests revealed that these residues did not affect the electrical conductivity properties of the composite materials [22].

### 3.3.3 BET-surface area analysis results

BET (Brunauer-Emmett-Teller) surface area analysis determines the specific surface area of porous samples by allowing nitrogen at –195.8°C to adsorb in multilayers on the sample surface. The surface area is quantified from the nitrogen adsorption quantity. The resulting value represents the mass-independent specific surface area. Nitrogen desorption subsequently occurs. Adsorption and desorption volumes are monitored across increasing relative pressures, $P/P_0$ where $P_0$ is the saturation pressure of nitrogen, to approach unity. The adsorption and desorption isotherms of the samples before (BF) and after (AF) washing are shown in Figure 5.

The adsorption-desorption isotherms in Figure 5 follow Type-II adsorption which occurs in non-porous materials like graphitic materials. A hysteresis loop at intermediate to high relative pressures is seen in Figure 5(a-c), indicating the presence of mesoporous structures and capillary condensation within inter-sheet spaces or slit-shaped pores of the exfoliated graphite [23]. The increased nitrogen adsorption capacity and enlarged hysteresis loop when the results of before and after washing were compared, suggest that washing generated additional accessible surface area and interlayer voids within the graphite structure.

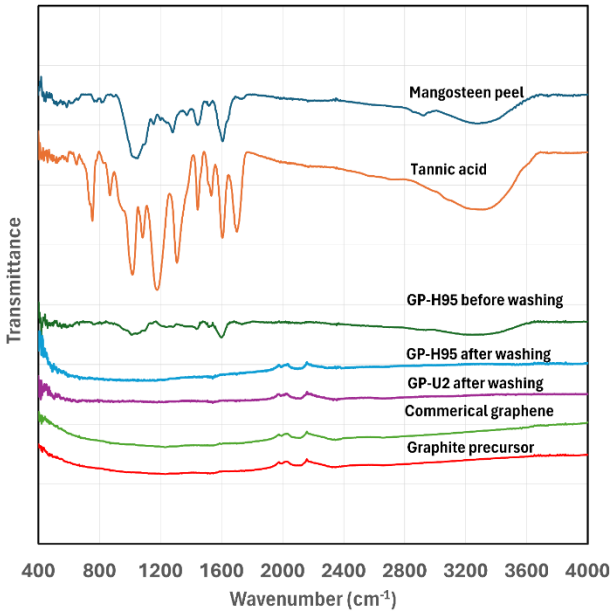


**Figure 4**. FTIR spectra of the graphite precursor, commercial graphene, mangosteen peel powder and tannic acid powder were compared with those of the exfoliated graphite before and after washing.

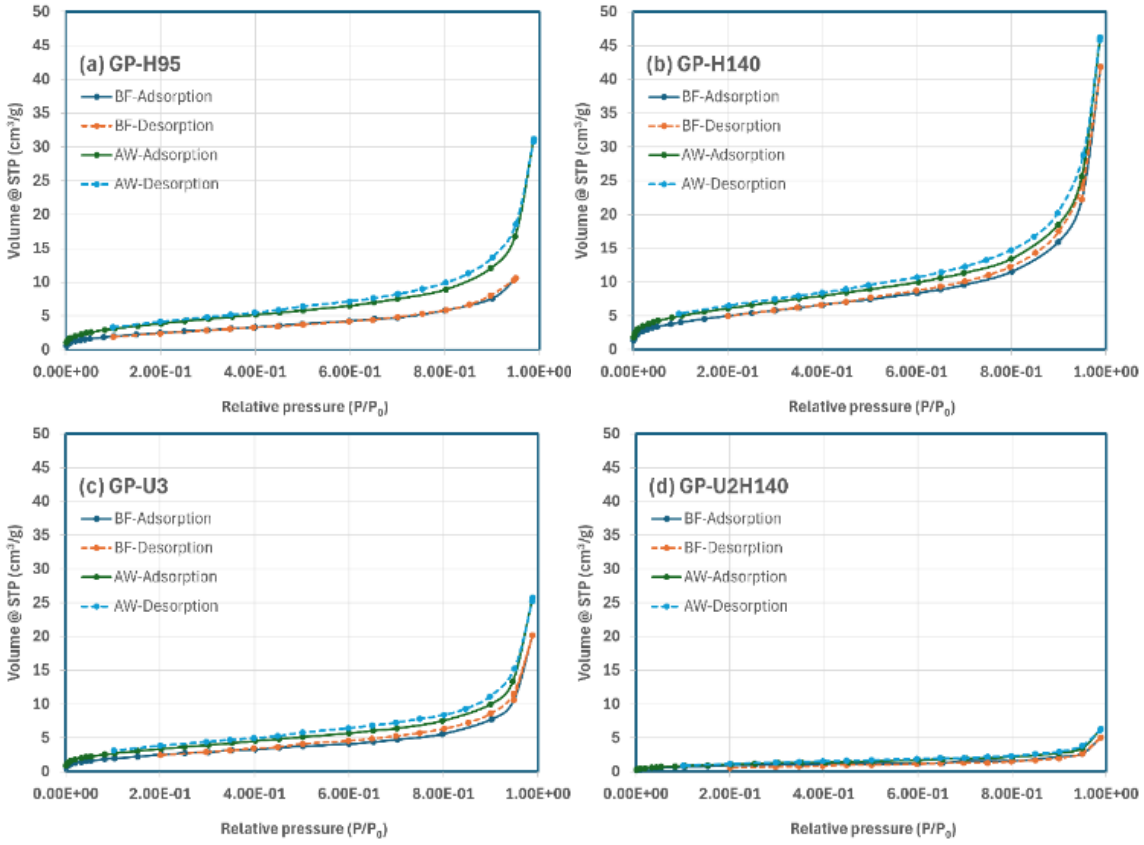


**Figure 5.** BET adsorption and desorption isotherms of the chosen exfoliated graphite samples.

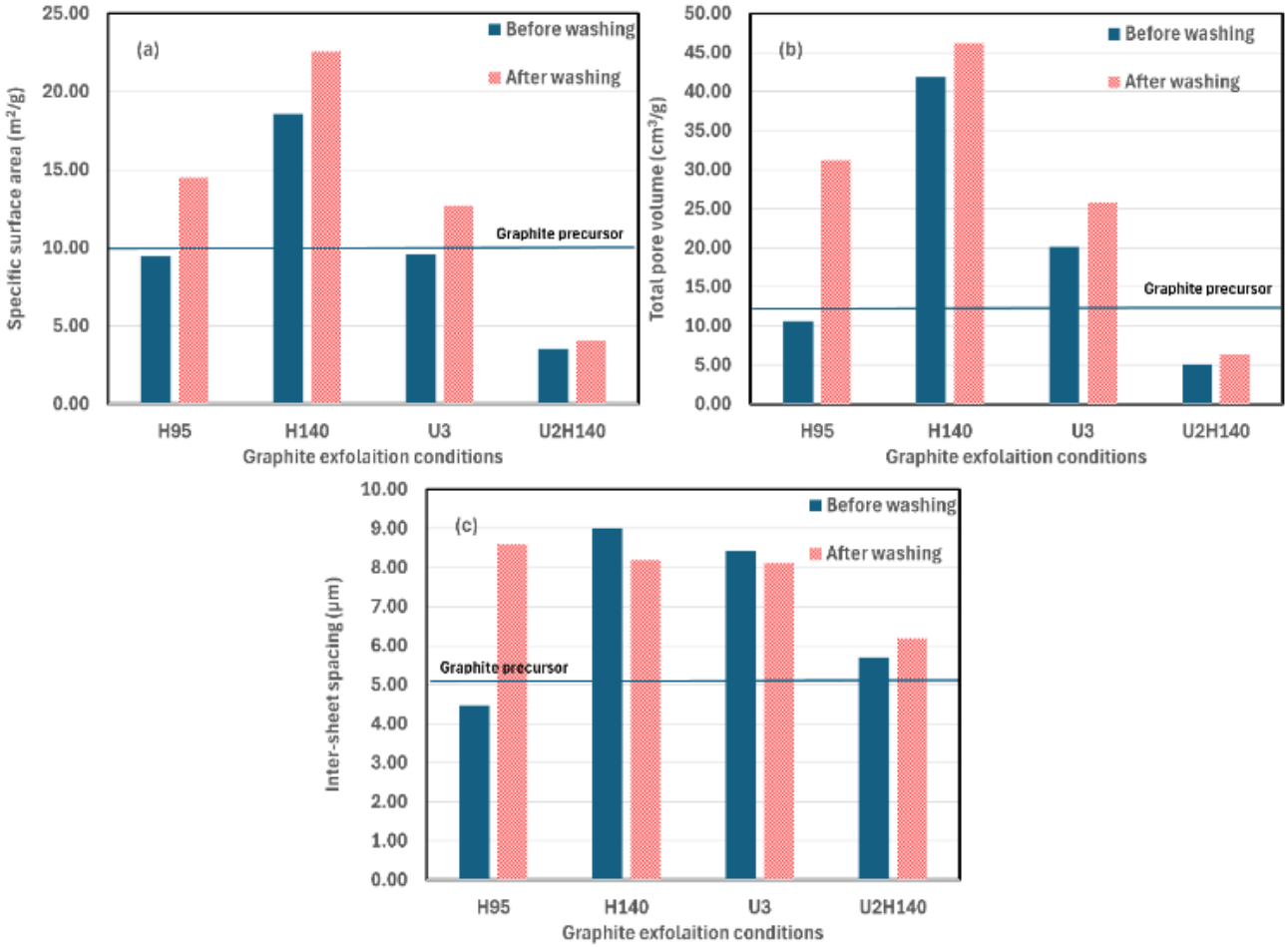


**Figure 6**. BET analysis results of the chosen exfoliated graphite samples compared with those of graphite precursor, represented by the reference lines.

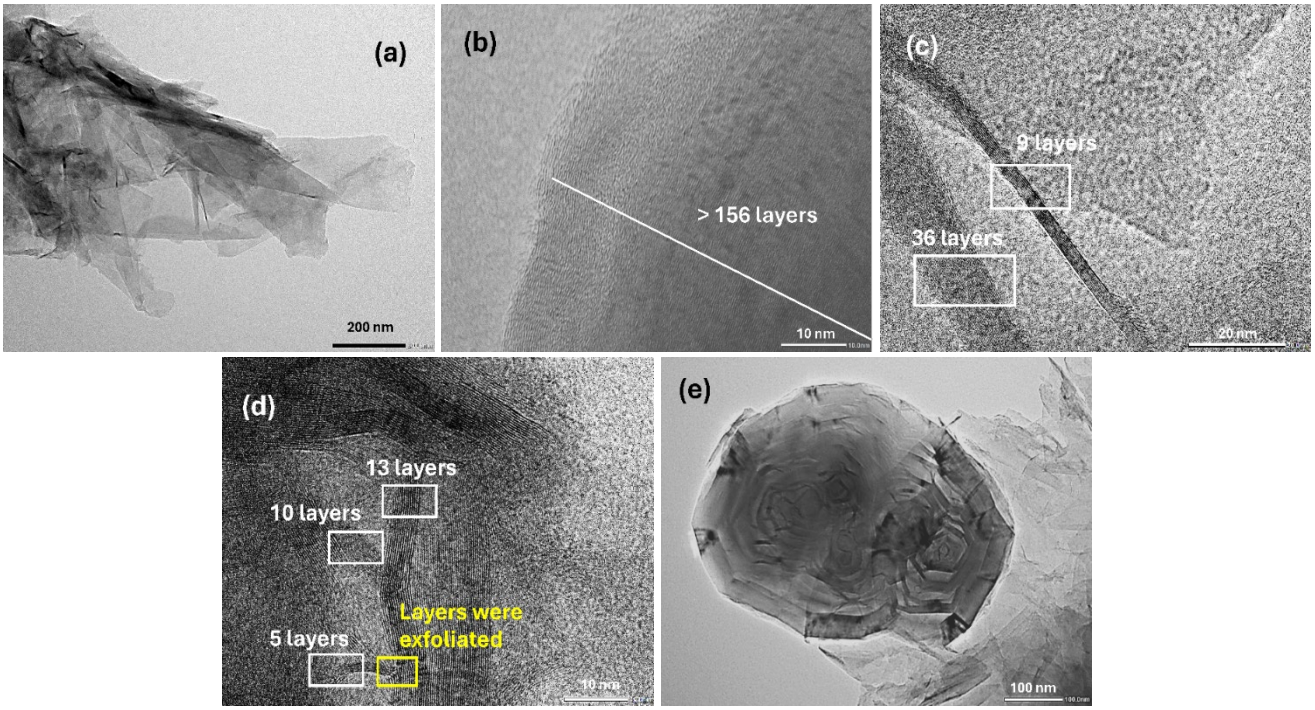


**Figure 7.** (a) TEM image of exfoliated graphite GP-U3 and HRTEM images of (b) unexfoliated graphite, (c) and (d) exfoliated samples containing five or more layers and (e) rose-like graphene structure.

The BET analysis results including specific surface area (SSA), total pore volume (Vp) and inter-sheet spacing could then be calculated and these are shown in Figure 6.

Figure 6(a) shows the specific surface area (SSA) of graphite at 10.11 $m^2 \cdot g^{-1}$ as the reference line, which is consistent with what was reported in other literatures for graphite powder with a particle size of 50 µm [23]. The BET analysis confirms that exfoliated graphite samples after washing have higher SSA and elevated total pore volumes ($V_p$) [24]. The maximum SSA was achieved at 22.55 $m^2 \cdot g^{-1}$ through homogenization at 14,000 rpm for 41 min, which corresponds to the lowest $I_{2D}$ /$I_G$ ratio observed in the single-step homogenization comparison.

Most of graphite exfoliation conditions yielded samples with SSA ranging from 12.69 $m^2 \cdot g^{-1}$ to 22.55 $m^2 \cdot g^{-1}$, which are higher than that of the graphite precursor, indicating total higher surface area due to exfoliation. It should be noted that GP-U2H140 has a lower SSA (4.09 $m^2 \cdot g^{-1}$) than the precursor graphite despite comparable average inter-sheet spacing. This anomaly as also shown in the adsorption-desorption isotherm that the sample adsorbed little amount of nitrogen even at the highest pressure applied and no hysteresis loop was seen. This suggests that there might be a high degree of aggregation of exfoliated graphite, probably due to the packing during drying process or bridge flocculation of organic molecules adsorbed on graphite surfaces, leading to a few accessible slit-shaped pores, impeding nitrogen adsorption and reducing the measured SSA.

### 3.3.4 Morphology of the exfoliated graphite

Transmission electron microscopy (TEM) was used to analyze the morphology of the exfoliated samples. TEM utilizes high-energy electron beams through very thin samples, enabling visualization of internal structures. High-resolution TEM (HRTEM) provides higher magnification which clearly shows the layer edges and allows layer counting in exfoliated samples [25].

Figure 7(a) illustrates the morphology of the exfoliated graphite GP-U3. It has thin sheet-like morphology with partial stacking overlap. With HRTEM mode, Figure 7(b) shows unexfoliated graphite with more than 156 layers while Figure 7(c-d) show multi-layer graphene or graphene-based materials which illustrate 5 layers or more similar to the structures of 8 layer to 9 layer of exfoliated graphite obtained from using ultra-high pressure at 20 MPa via jet cavitation method [23]. It is also possible for samples with large spatial sizes to fold as shown in Figure 7(e), which depicts rose-like graphene structure formed by folding of the graphene framework [26]. This indicates excellent exfoliation efficiency. The curved edges are smooth rather than sharp, indicating minimal defects [24]. These results are consistent with the lowest $I_D/I_G$ ratio obtained from the 2 h ultrasonic process.

## 3.4 Molecular dynamic simulation results

Molecular simulation uses computational methods to model molecular behavior in a force-field and predict macroscopic properties. It can be categorized into two main methodologies: stochastic methods (Monte Carlo simulations) and deterministic methods (Molecular Dynamics simulations). Molecular dynamics (MD) simulation is used to investigate time-dependent properties [27]. It averages properties over time intervals until equilibrium is reached.

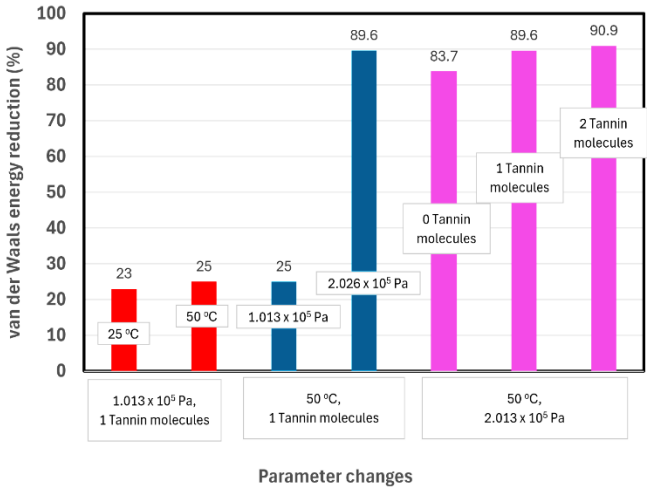


**Figure 8**. The van der Waals energy reduction (%) when parameters, including temperature, pressure and the number of tannin molecules, in the simulation were changed.

In Forcite module of BIOVIA Materials Studio program, the total potential energy is resulted from a combination of bond energy and non-bond energy. Non-bond energy consists of two parts including valence energy-cross terms (energy between atoms in the same molecule separated by more than 2 bonds) and intermolecular energy within the system. To simulate graphite exfoliation systems using condensed tannin solutions, the system consists of graphite, condensed tannin molecules and water molecules. Water molecules interact through dipole-dipole interactions, contributing to electrostatic energy (calculated from the interaction of partial charges). Graphite structure contains numerous C-C bonds in each layer and all layers interact through van der Waals forces. In a few-layer systems, adjacent layers show positive van der Waals energy due to electron cloud repulsion from the remaining electron of each carbon atom. The more distant layers have negative energy because they can attract each other within the specified cutoff distance following the Lennard-Jones potential energy model [28]. The summation of attractive and repulsive parts will be obtained as a resultant van der Waals energy. Therefore, if graphite layers moved away from one another, van der Waals energy of the whole system should be reduced. The reductions of van der Waals energy in cases of increasing temperature, increasing pressure and increasing the number of tannin molecules, when compared with the reference system of only graphite and water at 25°C and 1 atm which has the energy of 24,360 $kJ \cdot mol^{-1}$, are shown in Figure 8.

Figure 8 shows the results of molecular dynamics simulation of graphite exfoliation in condensed tannin solutions. Upon increasing the number of tannin molecules from 0 to 2, the reduction percentage of van der Waals energy is very large from 83.7% to 90.9%, indicating that the layers moved apart from each other at a far distant. Enhanced condensed tannin-graphite interactions facilitate exfoliation, subsequently diminishing electron cloud repulsion between graphite layers. Upon increasing pressure from $1.013 \times 10^5$ Pa to $2.026 \times 10^5$ Pa at 50°C resulted in the reduction percentage of van der Waals energy ranging from 25% to 86.9%. Increasing pressure in the simulated system resembles the actual process of sonication, where pressure from the bubble collapse have an impact on graphite edges. Even the breakup of bubbles occurring near graphite surfaces could increase

the pressure in vicinity which can affect the interaction among graphite layers. Finally, increasing temperature from 25°C to 50°C also shows the same effect of reduction of van der Waals energy of the system, indicating that increasing the temperature can also facilitate the graphite exfoliation. It is known that at higher temperature, the strength of interaction of molecules are weaken. This should affect both those of graphite-tannin molecules and those between graphite layers.

Some configurations of the simulated structures are shown in Figure 9–12, to show the exfoliation at 25°C and $1.013 \times 10^5$ Pa, at 50°C and $1.013 \times 10^5$ Pa, and at 50°C and $2.026 \times 10^5$ Pa using one tannin molecule, and at 50°C and $2.026 \times 10^5$ Pa using two condensed tannin molecules, respectively. Each figure shows the change of configurations at 0 ps, 7000 ps, 14000 ps and 200000 ps.

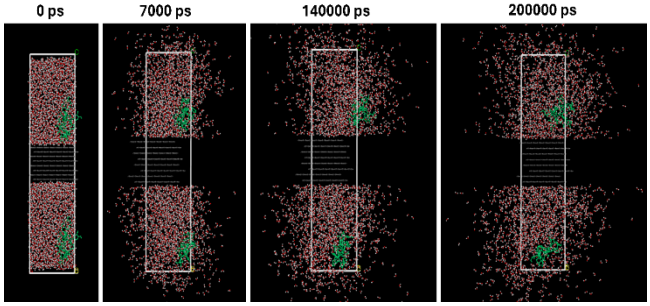


**Figure 9**. The layers of graphite moved away from one another at different times at 25°C and $1.013 \times 10^5$ Pa.

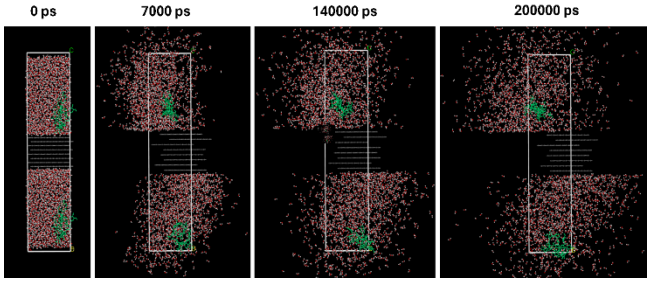


**Figure 10**. The layers of graphite moved away from one another at different times at 50°C and $1.013 \times 10^5$ Pa.

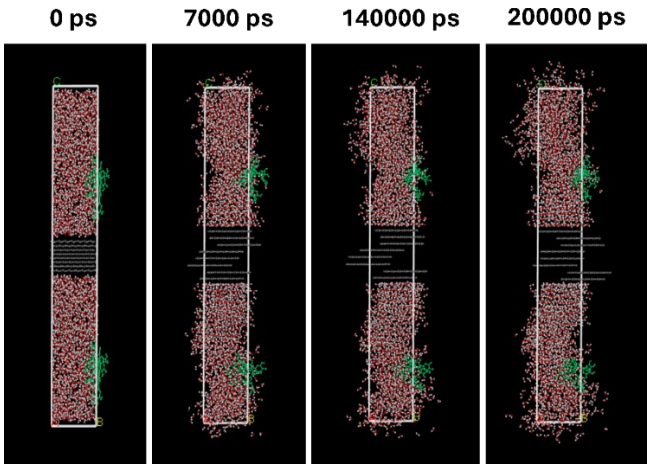


**Figure 11**. The layers of graphite moved away from one another at different times at 50°C and $2.026 \times 10^5$ Pa.

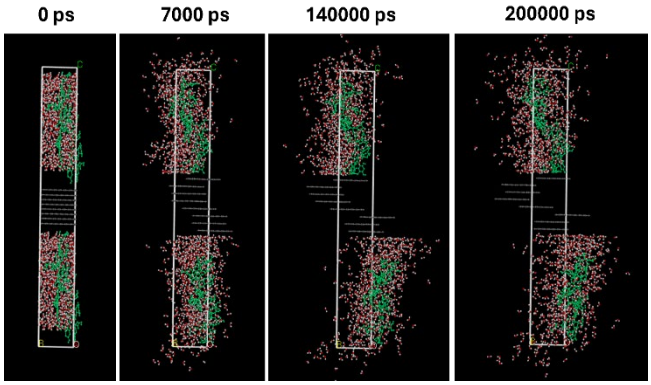


**Figure 12**. The layers of graphite moved away from one another at different times at 50°C and $2.026 \times 10^5$ Pa and using two condensed tannin molecules.

Even though the simulation results cannot directly explain the experiments of liquid phase exfoliation of graphite in this work, they can give the indirect evidence of graphite exfoliation considering both the results of van der Waals energy reduction and the final configurations of simulated systems. The temperature at 50°C is the condition we applied together with sonication (effect of cavitation pressure) in the ultrasound bath. The MD simulations showed that both increasing temperature and pressure could help facilitate the exfoliation and the presence of tannin molecules with many polyphenol groups could also benefit the exfoliation as hypothesized. However, the proof of the adsorption of tannin molecules on graphite surfaces and their π-π interaction should be clarified in the future using other modules in the BIOVIA program and other methods to simulate the systems representing the actual experiments.

## 4. Conclusions

The green graphite exfoliation using mangosteen-peel extract was successful in the system of applied shear forces (GP-H95 and GP-H140) and ultrasonication (GP-U2 and GP-U3) and sequential combinations of both methods (for example, GP-U3H140). Raman spectroscopy results confirmed that exfoliation truly occurred as the $I_{2D}/I_G$ ratios range from 0.51 to 0.55, significantly higher than that of graphite precursor and comparable to that of the commercial graphene-based product, indicating fewer layers. The GP-U3H140 sample presented the highest $I_{2D}/I_G$ due to successive external forces from ultrasonication and homogenization. The single-step process, GP-H140, yielded the sample with slightly lower $I_{2D}/I_G$ ratios than GP-U3H140 but higher than GP-U3.

The yield percentages of exfoliation processes ranged from 4.39% to 8.50%, surpassing previously reported values in a research work using tannic acid solution for graphite exfoliation [20]. Some two-step sequential processes (ultrasonication followed by homogenization) gave slight improvement in yield percentage and $I_{2D}/I_G$ ratios compared to single-step process. Molecular dynamics simulation revealed that when the change of van der Waals interaction was considered, increasing condensed tannin molecule concentration had the greatest effect on graphite exfoliation, followed by pressure and subsequently temperature.

All the results indicates that tannin adsorption, hydrodynamic shear, and cavitation pressure play different roles in graphite exfoliation.

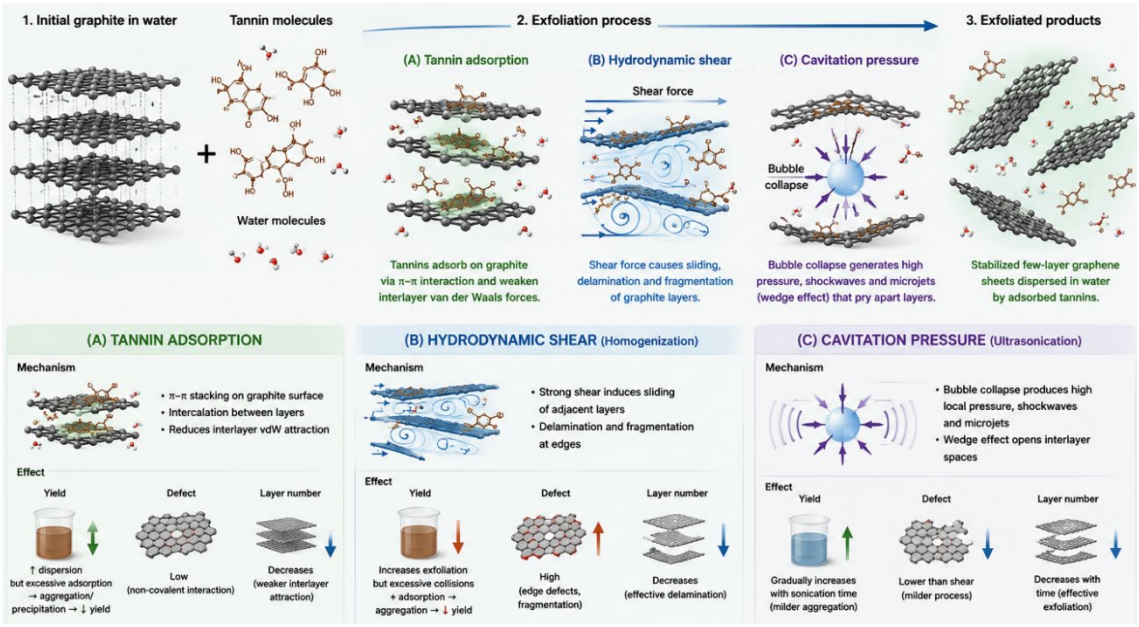


**Figure 13**. Schematic illustration of the proposed graphite exfoliation mechanism.

The mechanism is proposed as the following and shown in Figure 13. Condensed tannins adsorb onto graphite surfaces through π–π interactions, weakening interlayer van der Waals attraction and facilitating exfoliation. However, excessive adsorption may also promote aggregation and precipitation of graphite particles, thereby reducing the suspended yield. Hydrodynamic shear generated by homogenization promotes sliding and delamination of graphite layers, resulting in effective exfoliation but also producing more edge defects due to mechanical fragmentation. In contrast, cavitation pressure generated during ultrasonication exfoliates graphite through wedge effects induced by bubble collapse, leading to fewer structural defects and gradual reduction in layer number. Consequently, homogenization tends to produce samples with higher defect density, whereas ultrasonication provides milder exfoliation with lower defect formation.

Considering both quality (i.e. Raman spectroscopy results) and quantity (i.e. yield percentage) of the exfoliated graphite obtained in this study, the mangosteen-peel extract shows a great potential use in liquid phase exfoliation of graphite because it is an agricultural waste with low cost and contains a lot of phenolic contents. However, it is expected that it should be more effective when using an extract at a lower concentration to reduce the degree of adsorption in homogenization system. Our results show that adsorption of tannin molecules of graphite surfaces favors the exfoliation which is in competition with precipitation of the product. In addition, using an extract at a lower concentration should lower the cleaning load to obtain the clean products. This should be further studied in details in the future.

## Declaration of generative AI and AI-assisted technologies in the writing process

The authors utilize the ChatGPT tool in generating Figure 13 by supplying the results in this article to the program for the proposed mechanism of graphite exfoliation process.

## Acknowledgements

This study was supported by the Department of Chemical Engineering and Thammasat School of Engineering (TSE), the faculty of engineering, Thammasat university.

## References

[1] Y. Guo, X. Zuo, Y. Xue, J. Tang, M. Gouzman, Y. Fang, Y. Zhou, L. Wang, Y. Yu, and M. H. Rafailovich, "Engineering thermally and electrically conductive biodegradable polymer nanocomposites," *Composites Part B: Engineering*, vol. 189, p. 107905, 2020.

[2] T. Wang, C. Cheng, Z. Guan, T. Tao, Q. Xiao, and J. Zhu, "Chemical reduction-induced defect-rich bismuth oxide-reduced graphene oxide anode for high-performance supercapacitors," *Journal of Colloid and Interface Science*, vol. 677, pp. 45–54, 2025.

[3] M. P. Niharika, R. Garlapallya, K. Ruthvik, M. Velaga, and B. M. Rao, "Hydrogen production on g-$C_3N_4$ nanoflakes via photo-electrochemical water splitting," *Materials Today: Proceedings*, 2023,

[4] K. Ruthvik, A. Babu, P. Supraja, M. Navaneeth, V. Mahesh, K. U. Kumar, R. R. Kumar, B. M. Rao, D. Haranath, and K. Prakash, "High-performance triboelectric nanogenerator based on 2D graphitic carbon nitride for self-powered electronic devices," *Materials Letters*, vol. 350, p. 134947, 2023.

[5] T. Semangoen, R. Chotigawin, T. Sangnim, N. Chailerd, S. Yodkeeree, T. Pahasup-anan, and K. Huanbutta, "Antimicrobial efficacy of mangosteen (Garcinia mangostana) peel extracts in airborne microbial control within livestock farming environments," *Microbial Pathogenesis*, vol. 204, p. 107618, 2025.

[6] R. Li, B. S. Inbaraj, and B. Chen, "Quantification of xanthone

and anthocyanin in mangosteen peel by UPLC-MS/MS and preparation of nanoemulsions for studying their inhibition effects on liver cancer cells," *International Journal of Molecular Sciences*, vol. 24, p. 3934, 2023.

[7] M. M. Han, P. Tangpromphan, A. Kaewchada, and A. Jaree, "Recovery and partial isolation of α-mangostin from mangosteen pericarps via sequential extraction and precipitation," P*LoS One*, vol. 19, no. 10, p. e0310453, 2024.

[8] K. Moosophin, T. Wetthaisong, L. Seeratchakot, and W. Kokluecha, "Tannin extraction from mangosteen peel for protein precipitation in wine," in *Proceedings of the 3rd FerVAAP Conference*, vol. 15, no. 5, pp. 377–385, 2010.

[9] R. Navik, Y. Gai, W. Wang, and Y. Zhao, "Curcumin-assisted ultrasound exfoliation of graphite to graphene in ethanol," *Ultrasonics Sonochemistry*, vol. 48, pp. 96–102, 2018.

[10] U. T. Ferdous, A. Nurdin, S. Ismail, K. Shaari, and Z. N. Yusof, "A comparative study on antioxidant properties, total phenolics, total flavonoid contents, and cytotoxic properties of marine green microalgae and diatoms," *Journal of Genetic Engineering and Biotechnology*, vol. 23, no. 1, p. 100456, 2025.

[11] J. M. Monteiro, J. S. N. de Souza, E. M. F. Lins Neto, K. Scopel, and E. F. Trindade, "Does total tannin content explain the use value of spontaneous medicinal plants from the Brazilian semi-arid region?," *Revista Brasileira de Farmacognosia*, vol. 24, no. 2, pp. 116–123, 2014.

[12] T. P. Vo, D. N. Pham, T. V. Pham, H. Y. Nguyen, L. T. V. Vo, T. N. H. Tran, T. N. Tran, and D. Q. Nguyen, "Green extraction of total phenolic and flavonoid contents from mangosteen (Garcinia mangostana L.) rind using natural deep eutectic solvents," *Heliyon*, vol. 9, no. 4, p. e14884, 2023.

[13] A. Amiri, M. Naraghi, G. Ahmadi, M. Soleymaniha, and M. Shanbedi, "A review on liquid-phase exfoliation for scalable production of pure graphene, wrinkled, crumpled and functionalized graphene and challenges," *FlatChem*, vol. 8, pp. 40–71, 2018.

[14] S. Lund, J. Kauppila, S. Sirkia, J. Palosaari, O. Eklund, R. M. Latonen, J. H. Smått, J. Peltonen, and T. Lindfors, "Fast high-shear exfoliation of natural flake graphite with temperature control and high yield," *Carbon*, vol. 174, pp. 123–131, 2021.

[15] G. Liu, M. Xiao, X. Zhang, C. Gal, X. Chen, L. Liu, S. Pan, J. Wu, L. Tang, and D. Clements-Croome, "A review of air filtration technologies for sustainable and healthy building ventilation," *Sustainable Cities and Society*, vol. 32, pp. 375–396, 2017.

[16] Z. Li, L. Deng, I. A. Kinloch, and R. J. Young, "Raman spectroscopy of carbon materials and their composites: Graphene, nanotubes and fibres," *Progress in Materials Science*, vol. 135, p. 101089, 2023.

[17] A. Kaur, J. A. Morton, A. V. Tyurnina, A. Priyadarshi, M. Ghorbani, J. Mi, K. Porfyrakis, D. G. Eskin, and I. Tzanakis, "Dual frequency ultrasonic liquid phase exfoliation method for the production of few-layer graphene in green solvents," *Ultrasonics Sonochemistry*, vol. 108, p. 106954, 2024.

[18] N. Jirasitthanit, and P. Danwanichakul, "Increasing the yield in the exfoliation of graphite using serum from skim natural rubber latex in ultrasound-induced and shear-induced systems," *Engineering and Applied Science Research*, vol. 51, no. 1, pp. 42–49, 2024.

[19] S. Amloy, T. Lukprang, M. Lertworapreecha, and P. Preechaburana, "Green synthesis of carbon dots from mangosteen peel for fluorescent cancer cells," *Journal of Metals, Materials and Minerals*, vol. 34, p. 1957, 2024.

[20] Y. Kurniawan, M. Fahmi, and L. Yuliati, "Isolation and optical properties of natural pigments from purple mangosteen peels," *IOP Conference Series: Materials Science and Engineering*, vol. 833, p. 012018, 2020.

[21] T. Wahyono, D. Astuti, K. Wiryawan, I. Sugoro, and A. Jayanegara, "Fourier transform mid-infrared (FTIR) spectroscopy to identify tannin compounds in the panicle of sorghum mutant lines," *IOP Conference Series: Materials Science and Engineering*, vol. 546, p. 042045, 2019.

[22] S. Zhao, S. Xie, Z. Shicheng, Z. Zhao, J. Zhang, L. Li, and Z. Xin, "Green and high-efficiency production of graphene by tannic acid-assisted exfoliation of graphite in water," *ACS Sustainable Chemistry & Engineering*, vol. 6, no. 6, pp. 7652–7661, 2018.

[23] K. L. Ng, B. M. Maciejewska, L. Qin, C. Johnston, J. Barrio, M. M. Titirici, I. Tzanakis, D. G. Eskin, K. Porfyrakis, J. Mi, and N. Grobert, "Direct evidence of the exfoliation efficiency and graphene dispersibility of green solvents toward sustainable graphene production," *ACS Sustainable Chemistry & Engineering*, vol. 11, no. 1, pp. 58–66, 2023.

[24] K. Nuilek, W. Wongwiriyapan, V. Sattayarut, A. Simon, D. Koncz-Horváth, T. Ferenczi, F. Kristály, and P. Baumli, "Comparison of acid exfoliators in carbon nanosheets synthesis from stinging nettle (Urtica dioica) for electrochemical applications," *Scientific Reports*, vol. 10, no. 1, p. 17270, 2020.

[25] L. P. Chun, J. Y. Wu, and W. R. Liu, "Green and facile synthesis of few-layer graphene via liquid exfoliation process for lithium-ion batteries," *Scientific Reports*, vol. 8, p. 9766, 2018.

[26] Y. Hou, F. Qing, T. Wen, and X. Li, "Rose-like graphene as transmission electron microscopy support film," in Proceedings of the Ninth International Conference on Energy Materials and Electrical Engineering (ICEMEE 2023), 2024, p. 129791Q.

[27] J. J. de Groot, "Molecular dynamics simulation of atactic polystyrene using an all-atom model within materials studio," M.S. thesis, Eindhoven University of Technology, 2002.

[28] W. Cai, J. Li, B. P. Uberuaga, and S. Yip, "Molecular dynamics," in *Comprehensive Nuclear Materials*, 2nd ed., R. J. M. Konings and R. E. Stoller, Eds. Amsterdam, The Netherlands: Elsevier, 2020, pp. 573–594.